

Structure/activity relationships for the living Ziegler–Natta polymerization of 1-hexene by the series of cationic monocyclopentadienyl zirconium acetamidinate complexes, $[(\eta^5\text{-C}_5\text{Me}_5)\text{ZrMe}\{\text{N}(\text{CH}_2\text{R})\text{C}(\text{Me})\text{N}(\text{t-Bu})\}][\text{B}(\text{C}_6\text{F}_5)_4]$ (R = Me, i-Pr, t-Bu, Ph, 2-ClC₆H₄, 3-MeC₆H₄ and 2,4,6-Me₃C₆H₂)

Denis A. Kissounko, James C. Fettinger, Lawrence R. Sita*

Department of Chemistry and Biochemistry, University of Maryland, College Park, MD 20742, USA

Received 24 May 2002; accepted 23 July 2002

Dedicated to Professor Richard R. Schrock

Abstract

Protonation of $(\eta^5\text{-C}_5\text{Me}_5)\text{ZrMe}_2[\text{N}(\text{t-Bu})\text{C}(\text{Me})\text{N}(\text{CH}_2\text{R})]$ (**1**) [R = (a) Me, (b) i-Pr, (c) t-Bu, (d) Ph, (e) 2-ClC₆H₄, (f) 3-MeC₆H₄ and (g) 2,4,6-Me₃C₆H₂] by $[\text{PhNMe}_2\text{H}][\text{B}(\text{C}_6\text{F}_5)_4]$ in chlorobenzene at -10°C provides the titled cationic complexes **2a–g**. Both **2b** and **2d** are active initiators for the living polymerization of 1-hexene at -10°C , however, whereas **2d** functions much like **2a** in terms of activity and isoselectivity, propagation from **2b** is much less active and it produces atactic material. Complexes **2d** and **2g** are inactive, presumably due to steric reasons, while intramolecular chloride coordination appears responsible for inhibiting **2e**. Finally, **2f**, while active as an initiator, was found not to provide a living system as a result of C–H activation processes that terminate propagation. A structural study of the precatalysts **1b–d** sheds additional light on the nature of ligand effects on activity and stereocontrol for the family of initiators represented by **2**.

© 2002 Elsevier Science B.V. All rights reserved.

Keywords: Ziegler–Natta polymerization; Living polymerization; Poly(1-hexene); Amidinate complexes

1. Introduction

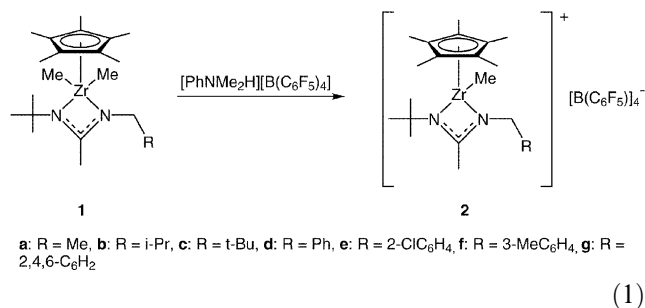
Following the initial reports of McConville and Scollard [1] and Schrock et al. [2], several groups have now similarly disclosed that certain classes of non-metallocene based Group 4 complexes can serve as initiators for the living Ziegler–Natta polymerization of propene and long chain α -olefins (e.g. 1-hexene) upon activation by either excess methylaluminumoxane (MAO) or a stoichiometric amount of a borane or borate cocatalyst [e.g. $\text{B}(\text{C}_6\text{F}_5)_3$ and $[\text{PhNMe}_2\text{H}][\text{B}(\text{C}_6\text{F}_5)_4]$, respectively] [3,4]. Some of these systems are also known to effect polymerization with a very high degree of stereocontrol, producing either an isotactic [3a,4] or

syndiotactic [3b,3c,3d] polymer microstructure. Regarding these efforts, we recently reported that activation of neutral dimethyl monocyclopentadienyl zirconium acetamidinates of the general structure, $(\eta^5\text{-C}_5\text{R}_5)\text{ZrMe}_2[\text{N}(\text{R}^1)\text{C}(\text{Me})\text{N}(\text{R}^2)]$ (**1**) (R = H or Me), by borate salts produces highly to extremely active cationic initiators for the living Ziegler–Natta polymerization of α -olefins and for the living cyclopolymerization of α,ω -non-conjugated dienes [4]. Importantly, depending upon the nature of the cyclopentadienyl groups, R, and the two acetamidinate substituents, R¹ and R², either a very high degree of stereocontrol could be achieved (i.e. isotactic when R = Me and R¹ ≠ R²) or none at all (i.e. R = H and/or R¹ = R²); except in the case of vinylcyclohexane where a highly isotactic microstructure is obtained regardless of the nature of the initiator, presumably due to stereocontrol by a chain-end control

* Corresponding author.

E-mail address: 15214@umail.umd.edu (L.R. Sita).

mechanism. In the specific example where $R = \text{Me}$, $R^1 = \text{Et}$, and $R^2 = t\text{-Bu}$ (**1a**), we have now determined, through extensive 2D NMR characterization of a purposefully synthesized low molecular weight, narrow polydispersity poly(1-hexene) sample ($M_n = 1800$, $M_w/M_n = 1.06$), that propagation proceeds in an isospecific (i.e. 100% stereoselective) and regiospecific (i.e. only 1,2-insertion) manner [5]. Accordingly, in this system, propagation must be proceeding through a single highly stereodifferentiating olefin binding site as opposed to the well established two-site stereocontrol model of zirconocenes [6]. This requirement, in turn, necessitates that rapid site-isomerization following olefin insertion must be occurring [7], and that epimerization of the zirconium center through ‘amidinate ring-flipping’ [8] must be far slower than propagation. Putting these processes together in terms of their relative rates, the following order must then be true: $k_{\text{iso}}[\text{Zr}] \gg k_{\text{p}}[\text{Zr}][\text{M}] \gg k_{\text{epi}}[\text{Zr}]$, where k_{iso} , k_{p} and k_{epi} are the respective rate constants for site-isomerization, propagation, and metal centered epimerization. Given that the magnitude of k_{iso} , k_{p} , and k_{epi} , and the degree of olefin face selectivity, should be dependent upon the steric bulk of the ligand environment about the metal center, we set out to map, in a systematic manner, the structure/activity relationships for the family of initiators derived from **1**. In the present work, we present the results of a study in which 1-hexene polymerization activity and degree of stereocontrol is correlated with a variation in the steric bulk of the ethyl substituent in **1a** through the additional synthesis and activation of the precatalysts **1b–g** shown in Eq. (1). As a part of this study, the solid-state geometrical parameters of three of these precatalysts, **1b–1d**, were compared to those previously reported for **1a** [4c].



a: $R = \text{Me}$, b: $R = i\text{-Pr}$, c: $R = t\text{-Bu}$, d: $R = \text{Ph}$, e: $R = 2\text{-ClC}_6\text{H}_4$, f: $R = 3\text{-MeC}_6\text{H}_4$, g: $R = 2,4,6\text{-C}_6\text{H}_2$

2. Experimental

2.1. General procedures

Manipulations were performed under an inert atmosphere of dinitrogen using standard Schlenk techniques or a vacuum atmospheres glovebox. Dry, oxygen-free

solvents were employed throughout. Diethyl ether (Et_2O), tetrahydrofuran (THF) and C_5H_{12} were distilled from Na/benzophenone (with a few milliliters of triglyme being added to the pot in the case of C_5H_{12}), and chlorobenzene (PhCl) was refluxed for several days over CaH_2 before being used for polymerizations. The monomer 1-hexene (99%) was obtained from Aldrich and stirred over NaK alloy (1:1) overnight before being vacuum-transferred. Benzene- d_6 was likewise vacuum transferred from NaK prior to being used for NMR spectroscopy. Chlorobenzene- d_5 was dried over CaH_2 prior to vacuum transfer. 1-(1,1-Dimethylethyl)-3-(2-methylpropyl)carbodiimide, 1-(1,1-dimethylethyl)-3-(2,2-dimethyl-propyl)carbodiimide, 1-(1,1-dimethylethyl)-3-benzylcarbodiimide, 1-(1,1-dimethylethyl)-3-(2-chlorobenzyl)carbodiimide, 1-(1,1-dimethylethyl)-3-(3-methyl-benzyl)carbodiimide and 1-(1,1-dimethylethyl)-3-(2,4,6-trimethylbenzyl)carbodiimide were all prepared through a previously published heterocumylene metathesis route [9]. $(\eta^5\text{-C}_5\text{Me}_5)\text{ZrCl}_3$ and $[\text{PhNMe}_2\text{H}][\text{B}(\text{C}_6\text{F}_5)_4]$ were obtained from Strem Chemicals and Boulder Scientific, respectively, and used without further purification.

GPC analyses were performed using a Waters GPC system equipped with a column oven and differential refractometer both maintained at 40°C and four columns (Waters Ultrastaygel 500 Å, Waters Styragel HR3, Waters Styragel HR4, and Shodex K-806M). THF was used as the eluant at a flow rate of 1.1 ml min^{-1} . M_n and M_w/M_n values were obtained using the Waters GPC software and seven different polystyrene standards (Polymer Laboratories). Elemental analyses were performed by Midwest Microlab Inc. ^1H and $^{13}\text{C}\{^1\text{H}\}$ NMR spectra were recorded at 400 and 100 MHz, respectively, using $\text{C}_6\text{H}_6\text{-d}_6$ or PhCl-d_5 as the solvent.

2.2. General procedure for the synthesis of $(\eta^5\text{-C}_5\text{Me}_5)\text{ZrMe}_2[\text{N}(\text{CH}_2\text{R})\text{C}(\text{Me})\text{N}(t\text{-Bu})]$ ($R = i\text{-Pr}$, $t\text{-Bu}$, Ph , $2\text{-ClC}_6\text{H}_5$, $3\text{-MeC}_6\text{H}_5$ and $2,4,6\text{-Me}_3\text{C}_6\text{H}_2$) (**1b–g**)

In the glovebox, 5.6 ml of methyl lithium (1.6 M in Et_2O), cooled to approximately -30°C in an internal refrigerator, was slowly added dropwise by pipette to a solution of 1.0 g (3 mmol) of $(\eta^5\text{-C}_5\text{Me}_5)\text{ZrCl}_3$ in 30 ml of Et_2O , also precooled to approximately -30°C . The reaction mixture was then allowed to warm to room temperature (r.t.) for 1 h, after which time, 3 mmol (neat) of the requisite carbodiimide was added by pipette. After stirring at r.t. for 12 h, the volatiles were removed in vacuo, the oily residue extracted by C_5H_{12} , the C_5H_{12} extract filtered through a glass frit and concentrated to a volume of approximately 3 ml. Overnight cooling of this solution at -30°C then afforded the desired complex as a white crystalline

material that was recrystallized to obtain analytically pure compound.

For compound **1b**: isolated yield 47%. ^1H NMR ($\text{C}_6\text{H}_6\text{-d}_6$, 25 °C): δ 0.15 (s, 6H, *ZrMe*); 0.75 (d, 6H, $J = 6.4$ Hz, *CHMe*₂); 1.12 (s, 9H, *CMe*₃); 1.61 (m, 1H, *CHMe*₂); 1.70 (s, 3H, *CMe*); 1.95 (s, 15H, *C*₅*Me*₅); 2.73 (s, 2H, *CH*₂). $^{13}\text{C}\{^1\text{H}\}$ NMR ($\text{C}_6\text{H}_6\text{-d}_6$, 25 °C): δ 11.6 (*CMe*₃); 15.7 (*ZrMe*); 20.4 (*CHMe*₂); 32.1 (*C*₅*Me*₅); 30.4 (*CH*₂); 45.3 (*CMe*); 52.6 (*CMe*₃); 55.1 (*CHMe*₂); 119.2 (*C*₅*Me*₅); 173.5 (*CMe*). *Anal. Calc.* for $\text{C}_{22}\text{H}_{42}\text{N}_2\text{Zr}$: C, 62.1; H, 9.9; N, 6.6. *Found*: C, 62.0; H, 9.9; N, 6.4%.

For compound **1c**: isolated yield 81%. ^1H NMR ($\text{C}_6\text{H}_6\text{-d}_6$, 25 °C): δ 0.21 (s, 6H, *ZrMe*); 0.80 (s, 9H, *CH*₂*CMe*₃); 1.13 (s, 9H, *CMe*₃); 1.74 (s, 3H, *CMe*); 1.93 (s, 15H, *C*₅*Me*₅); 2.85 (s, 2H, *CH*₂). $^{13}\text{C}\{^1\text{H}\}$ NMR ($\text{C}_6\text{H}_6\text{-d}_6$, 25 °C): δ 11.8 (*CMe*₃); 16.3 (*ZrMe*); 28.6 (*CH*₂*CMe*₃); 32.3 (*C*₅*Me*₅); 33.2 (*CH*₂); 46.9 (*CMe*); 53.1 (*CMe*₃); 58.2 (*CH*₂*CMe*₃); 119.1 (*C*₅*Me*₅); 173.8 (*CMe*). *Anal. Calc.* for $\text{C}_{23}\text{H}_{44}\text{N}_2\text{Zr}$: C, 62.8; H, 10.1; N, 6.4. *Found*: C, 62.9; H, 10.1; N, 6.2%.

For compound **1d**: isolated yield 53%. ^1H NMR ($\text{C}_6\text{H}_6\text{-d}_6$, 25 °C): δ 0.20 (s, 6H, *ZrMe*); 1.11 (s, 9H, *CMe*₃); 1.60 (s, 3H, *CMe*); 1.93 (s, 15H, *C*₅*Me*₅); 4.13 (s, 2H, *CH*₂); 7.10–7.13 (m, 5H, *C*₆*H*₅). $^{13}\text{C}\{^1\text{H}\}$ NMR ($\text{C}_6\text{H}_6\text{-d}_6$, 25 °C): δ 11.5 (*CMe*₃); 16.0 (*ZrMe*); 31.8 (*C*₅*Me*₅); 44.6 (*CMe*); 50.7 (*CH*₂); 52.7 (*CMe*₃); 119.5 (*C*₅*Me*₅); 126.0–142.7 (*C*₆*H*₅); 174.6 (*CMe*). *Anal. Calc.* for $\text{C}_{25}\text{H}_{40}\text{N}_2\text{Zr}$: C, 65.3; H, 8.8; N, 6.1. *Found*: C, 65.5; H, 8.8; N, 6.0%.

For compound **1e**: isolated yield 67%. ^1H NMR ($\text{C}_6\text{H}_6\text{-d}_6$, 25 °C): δ 0.22 (s, 6H, *ZrMe*); 1.10 (s, 9H, *CMe*₃); 1.51 (s, 3H, *CMe*); 1.89 (s, 15H, *C*₅*Me*₅); 4.33 (s, 2H, *CH*₂); 6.72–7.30 (m, 4H, *C*₆*H*₄). $^{13}\text{C}\{^1\text{H}\}$ NMR ($\text{C}_6\text{H}_6\text{-d}_6$, 25 °C): δ 11.4 (*CMe*₃); 15.5 (*ZrMe*); 31.8 (*C*₅*Me*₅); 45.1 (*CMe*); 48.5 (*CH*₂); 52.7 (*CMe*₃); 119.6 (*C*₅*Me*₅); 123.1–139.7 (*C*₆*H*₄); 175.0 (*CMe*). *Anal. Calc.* for $\text{C}_{25}\text{H}_{39}\text{ClN}_2\text{Zr}$: C, 60.8; H, 8.0; N, 5.7. *Found*: C, 60.7; H, 7.9; N, 5.7%.

For compound **1f**: isolated yield 46%. ^1H NMR ($\text{C}_6\text{H}_6\text{-d}_6$, 25 °C): δ 0.21 (s, 6H, *ZrMe*); 1.12 (s, 9H, *CMe*₃); 1.64 (s, 3H, *CMe*); 1.94 (s, 15H, *C*₅*Me*₅); 2.12 (s, 3H, *C*₆*H*₄*Me*); 4.14 (s, 2H, *CH*₂); 6.83–67.11 (m, 4H, *C*₆*H*₄). $^{13}\text{C}\{^1\text{H}\}$ NMR ($\text{C}_6\text{H}_6\text{-d}_6$, 25 °C): δ 11.5 (*CMe*₃); 16.0 (*ZrMe*); 21.1 (*C*₆*H*₄*Me*); 31.8 (*C*₅*Me*₅); 44.6 (*CMe*); 50.6 (*CH*₂); 52.7 (*CMe*₃); 119.5 (*C*₅*Me*₅); 123.1–142.5 (*C*₆*H*₄); 174.7 (*CMe*). *Anal. Calc.* for $\text{C}_{26}\text{H}_{42}\text{N}_2\text{Zr}$: C, 65.9; H, 8.9; N, 5.9. *Found*: C, 65.72; H, 8.91; N, 5.87%.

For compound **1g**: isolated yield 54%. ^1H NMR ($\text{C}_6\text{H}_6\text{-d}_6$, 25 °C): δ 0.17 (s, 6H, *ZrMe*); 1.18 (s, 9H, *CMe*₃); 1.70 (s, 3H, *CMe*); 1.85 (s, 15H, *C*₅*Me*₅); 2.10 (s, 3H, *p-MeC*₆*H*₂); 2.22 (s, 6H, *o-MeC*₆*H*₂); 4.18 (s, 2H, *CH*₂); 6.74 (s, 2H, *C*₆*H*₂). $^{13}\text{C}\{^1\text{H}\}$ NMR ($\text{C}_6\text{H}_6\text{-d}_6$, 25 °C): δ 11.4 (*CMe*₃); 16.4 (*ZrMe*); 20.5 (*p-MeC*₆*H*₂); 20.6 (*o-MeC*₆*H*₂); 32.0 (*C*₅*Me*₅); 44.9 (*CMe*); 47.2 (*CH*₂); 52.9 (*CMe*₃); 119.5 (*C*₅*Me*₅); 127.4, –136.3

(*C*₆*H*₂); 172.4 (*CMe*). *Anal. Calc.* for $\text{C}_{28}\text{H}_{46}\text{N}_2\text{Zr}$: C, 67.0; H, 9.2; N, 5.6. *Found*: C, 67.1; H, 9.2; N, 5.5%.

2.3. General procedure for in situ generation of initiators **2b–g** and polymerization of 1-hexene

Within the internal refrigerator of a glovebox, maintained at –10 °C and equipped with a low profile mini magnetic stirrer, the precatalyst, **1b** (0.02 mmol) was dissolved in 2 ml of PhCl within a glass vial. In a separate vial, 0.016 g (0.02 mmol) of [PhNHMe₂]-[B(C₆F₅)₄] (cocatalyst) was dissolved in 8 ml of PhCl. After cooling to –10 °C, the solution of precatalyst was added rapidly by pipette to the cocatalyst to give a clear yellow solution of the corresponding cationic species **2b**. To this rapidly stirred solution of initiator, 0.55 ml (4 mmol) of 1-hexene was then rapidly added all at once and the reaction mixture was stirred at –10 °C for 2 h, whereupon it was quenched by the addition of silica gel (degassed). After filtering, all the volatiles were removed in vacuo, the oily residue redissolved in approximately 5 ml of CHCl₃ and the poly(1-hexene) precipitated by dropwise addition into 400 ml of acidified (HCl) MeOH. The purified polymer was then isolated and dried overnight at 70 °C/0.01 mmHg.

For obtaining the ^1H NMR spectra of the initiators, **2b–g**, a solution of the precatalyst (0.02 mmol in approximately 0.5 ml of PhCl-d₅, was added to a suspension of 16 mg (0.02 mmol) of [PhNHMe₂]-[B(C₆F₅)₄] in approximately 0.5 ml of PhCl-d₅, also precooled to –10 °C. The resulting clear yellow solution of the corresponding cationic species was then transferred to a NMR tube that was kept cooled to –10 °C in a dewar before being inserted into the NMR probe that was maintained at the same temperature.

2.4. Crystal structure determinations

Data was collected on a Bruker SMART CCD system operating at –80 °C. All crystallographic calculations were performed on a Personal computer (PC) with a Pentium 1.80 GHz processor and 512 MB of extended memory. The SHELXTL program package was implemented to determine the probable space group and set up the initial files. Table 1 provides information on the data collection and refinement parameters for compounds **1b–d**.

2.4.1. Crystal structure determination of compound **1b**

A colorless plate with approximate orthogonal dimensions 0.492 × 0.306 × 0.092 mm³ was placed and optically centered on the Bruker SMART CCD system at –80 °C. The initial unit cell was indexed using a least-squares analysis of a random set of reflections collected from three series of 0.3° wide ω -scans, 10 s per frame, and 25 frames per series that were well distributed in

Table 1
Crystallographic data and details of refinement for compounds **1b–d**

	1b	1c	1d
Empirical formula	C ₂₂ H ₄₂ N ₂ Zr	C ₂₃ H ₄₄ N ₂ Zr	C ₂₅ H ₄₀ N ₂ Zr
Formula weight	425.80	439.82	459.81
Temperature (K)	193(2)	193(2)	193(2)
Crystal system	triclinic	monoclinic	monoclinic
Space group	<i>P</i> $\bar{1}$	<i>P</i> 2 ₁ / <i>c</i>	<i>P</i> 2 ₁ / <i>c</i>
<i>a</i> (Å)	8.7213(4)	15.9229(6)	8.5629(5)
<i>b</i> (Å)	9.8836(4)	17.7627(6)	29.7302(16)
<i>c</i> (Å)	14.5957(6)	17.6180(6)	10.1619(6)
α (°)	72.8290(10)	90	90
β (°)	76.9400(10)	100.3150(10)	106.1140(10)
γ (°)	82.8010(10)	90	90
<i>V</i> (Å ³)	1168.63(9)	4902.4(3)	2485.3(2)
<i>Z</i>	2	8	4
ρ_{calc} (g cm ⁻³)	1.210	1.192	1.229
μ (Mo) (mm ⁻¹)	0.477	0.457	0.454
Crystal size (mm)	0.492 × 0.306 × 0.092	0.607 × 0.388 × 0.286	0.617 × 0.274 × 0.108
2 θ Range (°)	2.26–27.49	1.64–27.50	2.20–27.50
Total reflections	18 551	78 069	39 635
Independent reflections	5330 [<i>R</i> _{int} = 0.0182]	11 257 [<i>R</i> _{int} = 0.0269]	5712 [<i>R</i> _{int} = 0.0379]
Data/restraints/parameters	5330/3/398	11 257/6/828	5712/3/417
Final <i>R</i> indices [<i>I</i> > 2 σ (<i>I</i>)]	<i>R</i> ₁ = 0.0215, <i>wR</i> ₂ = 0.0575	<i>R</i> ₁ = 0.0322, <i>wR</i> ₂ = 0.0871	<i>R</i> ₁ = 0.0307, <i>wR</i> ₂ = 0.0832
<i>R</i> indices (all data)	<i>R</i> ₁ = 0.0245, <i>wR</i> ₂ = 0.0596	<i>R</i> ₁ = 0.0391, <i>wR</i> ₂ = 0.0924	<i>R</i> ₁ = 0.0416, <i>wR</i> ₂ = 0.0902
Goodness-of-fit	1.098	1.079	1.086

reciprocal space. Data frames were collected [Mo K α] with 0.3° wide ω -scans, 14 s per frame and 606 frames per series. Five complete series were collected at varying ϕ angles ($\phi = 0, 72, 144, 216, 288^\circ$). The crystal to detector distance was 4.888 cm, thus providing a complete sphere of data to $2\theta_{\text{max}} = 50.0^\circ$. A total of 18 551 reflections were collected and corrected for Lp effects and absorption using Blessing's method as incorporated into the program SADABS [1,2] with 5330 unique [*R*_{int} = 0.0192]. System symmetry, lack of systematic absences and intensity statistics indicated the chiral triclinic space group *P*1 (no. 1); however the centric triclinic space group *P* $\bar{1}$ (no. 2) was chosen. The structure was determined by direct methods with the successful location of nearly all non-hydrogen atoms using the program xs [4]. The structure was refined with XL [5]. One least-squares difference-Fourier cycle was required to locate the remaining non-hydrogen atoms. All non-hydrogen atoms were refined anisotropically. The hydrogen atoms were initially placed in calculated positions but allowed to refine freely during the final stages of refinement (*xyzU*). The final structure was refined to convergence [$\Delta/\sigma \leq 0.002$] with *R*(*F*) = 2.45%, *wR*(*F*²) = 5.96%, GOF = 1.098 for all 5330 unique reflections [*R*(*F*) = 2.15%, *wR*(*F*²) = 5.75% for those 4951 data with *F*_o > 4 σ (*F*_o)]. The final difference-Fourier map was featureless indicating that the structure is both correct and complete.

2.4.2. Crystal structure determination of compound **1c**

A colorless irregular block with approximate orthogonal dimensions 0.607 × 0.388 × 0.286 mm³ was placed and optically centered on the diffractometer. The initial unit cell was indexed using a least-squares analysis of a random set of reflections collected from three series of 0.3° wide ω -scans, 10 s per frame, and 25 frames per series that were well distributed in reciprocal space. Data frames were collected [Mo K α] with 0.3° wide ω -scans, 10 s per frame and 606 frames per series. Five complete series were collected at varying ϕ angles ($\phi = 0, 72, 144, 216, 288^\circ$). An additional 200 frames, a repeat of the first series for redundancy and decay purposes, were also collected. The crystal to detector distance was 4.813 cm, thus providing a complete sphere of data to $2\theta_{\text{max}} = 55.0^\circ$. A total of 78 069 reflections were collected and corrected for Lp effects and absorption using Blessing's method as incorporated into the program SADABS with 11 257 unique [*R*_{int} = 0.0269]. System symmetry, systematic absences and intensity statistics indicated the unique centric monoclinic space group *P*2₁/*c* (no. 14). The structure was determined by direct methods with the successful location of nearly all non-hydrogen atoms using the program xs. The structure was refined with XL. One least-squares difference-Fourier cycle was required to locate the remaining non-hydrogen atoms. All non-hydrogen atoms were refined anisotropically. Hydrogen atoms were initially placed in calculated positions; then allowed to refine freely during

the final refinement stages. The final structure was refined to convergence [$\Delta/\sigma \leq 0.003$] with $R(F) = 3.91\%$, $wR(F^2) = 9.24\%$, $GOF = 1.079$ for all 11 257 unique reflections [$R(F) = 3.22\%$, $wR(F^2) = 8.71\%$ for those 9832 data with $F_o > 4\sigma(F_o)$]. The final difference-Fourier map possessed one large peak, $1.25 \text{ e}/\text{\AA}^2$, within 0.8 \AA of the central Zr(1), labeled atom while the remainder of the map was featureless indicating that the structure is both correct and complete.

2.4.3. Crystal structure determination of compound **1d**

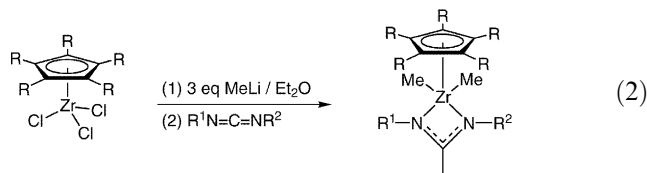
A colorless plate with approximate orthogonal dimensions $0.617 \times 0.274 \times 0.108 \text{ mm}^3$ was placed and optically centered on the diffractometer. The initial unit cell was indexed using a least-squares analysis of a random set of reflections collected from three series of 0.3° wide ω -scans, 10 s per frame, and 25 frames per series that were well distributed in reciprocal space. Data frames were collected [$\text{Mo K}\alpha$] with 0.3° wide ω -scans, 16 s per frame and 606 frames per series. Five complete series were collected at varying ϕ angles ($\phi = 0, 72, 144, 216, 288^\circ$). An additional 200 frames, a repeat of the first series for redundancy and decay purposes, were also collected. The crystal to detector distance was 4.813 cm , thus providing a complete sphere of data to $2\theta_{\text{max}} = 55.0^\circ$. A total of 39 635 reflections were collected and corrected for Lp effects and absorption using Blessing's method as incorporated into the program SADABS with 5712 unique [$R_{\text{int}} = 0.0379$]. System symmetry, systematic absences and intensity statistics indicated the unique centric monoclinic space group $P2_1/c$ (no. 14). The structure was determined by direct methods with the successful location of nearly all non-hydrogen atoms using the program xs. The structure was refined with XL. One least-squares difference-Fourier cycle was required to locate the remaining non-hydrogen atoms. All non-hydrogen atoms were refined anisotropically. Hydrogen atoms were initially placed in calculated positions; then allowed to refine freely during the final refinement stages. A centroid for the pentamethylcyclopentadienyl ligand was calculated. The final structure was refined to convergence [$\Delta/\sigma \leq 0.001$] with $R(F) = 4.16\%$, $wR(F^2) = 9.02\%$, $GOF = 1.086$ for all 5712 unique reflections [$R(F) = 3.07\%$, $wR(F^2) = 8.32\%$ for those 4725 data with $F_o > 4\sigma(F_o)$]. The final difference-Fourier map was featureless indicating that the structure is both correct and complete.

3. Results and discussion

3.1. Preparation of precatalysts **1b–g**

As previously described, neutral dimethyl monocyclopentadienyl zirconium acetamidinates of the general formula, $(\eta^5\text{-C}_5\text{R}_5)\text{ZrMe}_2[\text{N}(\text{R}^1)\text{C}(\text{Me})\text{N}(\text{R}^2)]$, can be

conveniently prepared in high yield through carbodiimide insertion into a zirconium–methyl bond of $(\eta^5\text{-C}_5\text{R}_5)\text{ZrMe}_3$ that is generated in situ from the corresponding $(\eta^5\text{-C}_5\text{R}_5)\text{ZrCl}_3$ reagent according to Eq. (2) [4a,4d,8]. Furthermore, the required carbodiimide for this process, if not commercially available, can be readily obtained through a tin(II)-mediated heterocumulene metathesis between a *N*-trimethylsilyl amine, $\text{R}^1\text{NH}(\text{SiMe}_3)$, and an isocyanate, R^2NCO [9]. For the present study, the precatalysts **1b–g** were all obtained through this carbodiimide insertion route in unoptimized isolated yields ranging from 45 to 81% as analytically pure white crystalline materials.



3.2. Crystal structures of compounds **1b–d**

As it has proven not to be routinely possible to obtain single crystals of the cationic initiators themselves, we sought to examine what consequences an increase in the steric bulk of the ethyl substituent of **2a** might have on the nature of bonding of the monocyclopentadienyl/acetamidinate ligand set within the series of new cationic species, **2b–g**, by comparing the geometrical parameters obtained for the precatalysts **1b–d** with those previously obtained for the precatalyst **1a** [4c]. Figs. 1–3 present the molecular structures for compounds **1b–d**, respectively, as obtained from single-crystal X-ray crystallographic analyses, and Table 2 provides selected geometrical parameters as derived from these structures.

Using the geometrical parameters of **1a** as a benchmark, several key features of the molecular structures of

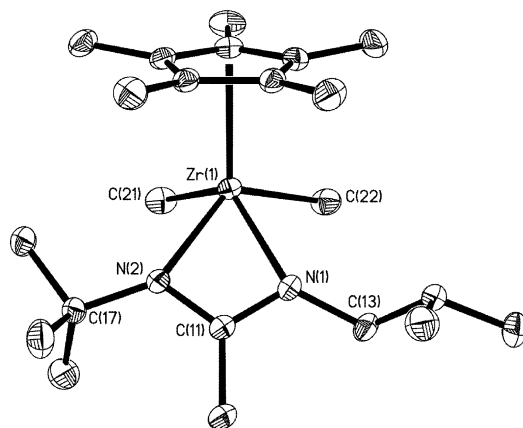


Fig. 1. Molecular structure of compound **1b** (30% thermal ellipsoids). Hydrogen atoms have been removed for the sake of clarity.

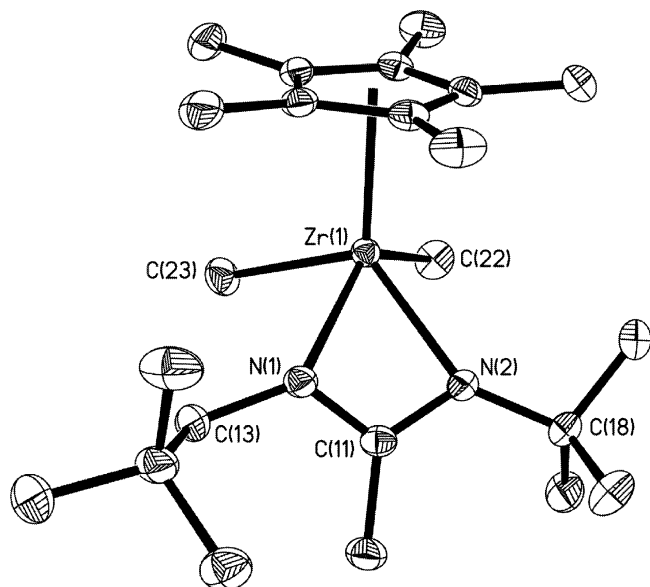


Fig. 2. Molecular structure of compound **1c** (30% thermal ellipsoids). Hydrogen atoms have been removed for the sake of clarity.

1b–d can be pointed out. To begin, the most obvious differences are to be found between compounds **1a** and **1c**, presumably as a result of a significant increase in non-bonded steric interactions between substituents of the latter. For instance, the Zr(1)–N(1) bond distance of **1c** is considerably longer at 2.3234(15) Å than the corresponding distance of 2.251(3) Å in **1a**. The nitrogen atom that bears the neopentyl group in **1c**, N(1), is also substantially more pyramidalized than the nitrogen atom in **1a** that bears the ethyl group as revealed by a comparison of the sum of the bond angles about each nitrogen atom (c.f. $\Sigma \theta_{N(1)} = 353.52$ vs. 343.512° in **1a** and **1c**, respectively). In contrast, both the Zr(1)–N(1) bond distances and the $\Sigma \theta_{N(1)}$ values for **1b** and **1d**, 2.251 Å, 353.62° and 2.552(17) Å; 353.27° , respectively, are very similar to the corresponding values found for

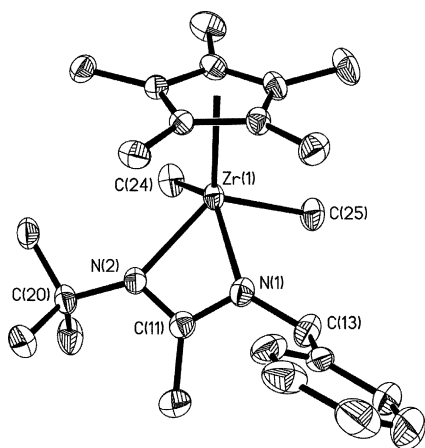


Fig. 3. Molecular structure of compound **1d** (30% thermal ellipsoids). Hydrogen atoms have been removed for the sake of clarity.

1a. For the nitrogen atom bearing the *t*-butyl group, N(2), once more the $\Sigma \theta_{N(2)}$ values are nearly identical for **1a** and **1d**, 357.26 and 357.68° , respectively, whereas in **1b** and **1c**, it is somewhat smaller at 356.2 and 356.47° , respectively. A final consequence of strong non-bonded interactions that is evident in the molecular structure of **1c** is the significant degree of non-planarity displayed by the four-membered ring of the amidinate fragment as measured by the angle between the planes defined by Zr(1)–N(1)–C(11) and Zr(1)–N(2)–C(11). In **1c**, this ‘envelope’ angle is 33.6° , whereas in **1a** and **1d**, it is nearly identical at 18.3 and 18.1° , respectively. Interestingly, the corresponding value for **1b** is the smallest at only 14.9° . In summary then, while the molecular structure of **1d** is virtually identical to **2a** with respect to these specific geometrical parameters, that of **1c** is quite different and **1b** is closer to **1a** than to **1c**.

3.3. Solution configurational stabilities of precatalysts **1b–g** and cationic initiators **2b–g**

In keeping with previous observations [4], the C_1 -symmetric precatalysts **1b–g** are all configurationally unstable in solution at room temperature with respect to racemization of the zirconium center that occurs through a facile amidinate ring-flipping process that serves to exchange the diastereotopic methylene protons of the N–CH_aH_bR substituent. For precatalyst **1a**, the barrier to this racemization process, ΔG_c^\ddagger , was previously found to be only $10.9 \text{ kcal mol}^{-1}$ at a low T_c of 223 K [4c], and therefore, it is clear that even a substantial increase in steric bulk of the N–CH₂R group, such as that presented by **1c**, does not serve to raise this barrier significantly.

In contrast to the configurational instability of the precatalysts, the cationic initiators **2b–d** were all found to be *configurationally stable* at -10°C on the NMR timeframe as indicated by diagnostic resonances with narrow line widths now being observed for the diastereotopic protons mentioned above. Fig. 4 presents the ¹H NMR spectrum for **2d** where these diastereotopic resonances show up as an AB quartet (see inset). Surprisingly, the cationic species **2e**, which has a 2-chlorobenzyl substituent, was found to be *configurationally unstable* by ¹H NMR spectroscopy down to -30°C , which is the temperature limit of the solvent. The origin of this difference in configurational stability between **2d** and **2e** may be due to the ability of the 2-chlorobenzyl substituent to alleviate the electron deficiency of the cationic zirconium center through an intramolecular coordination of the chlorine atom to zirconium, thereby, decreasing the barrier to amidinate ring-flipping through a lengthening of zirconium–nitrogen bonds. Finally, similar ¹H NMR studies of **2f** and **2g** found that these initiators are *chemically unstable* at -10°C , potentially as a result of facile C–H activation

Table 2
Selected bond distances (Å) and angles (°) for compounds **1a–d**

1b		1c		1d	
<i>Bond distances</i>					
Zr(1)–N(1)	2.2465(11)	Zr(1)–N(1)	2.3234(15)	Zr(1)–N(1)	2.2552(17)
Zr(1)–N(2)	2.2829(11)	Zr(1)–N(2)	2.2439(15)	Zr(1)–N(2)	2.2910(16)
Zr(1)–C(21)	2.2714(16)	Zr(1)–C(22)	2.269(2)	Zr(1)–C(22)	2.274(2)
Zr(1)–C(22)	2.2717(16)	Zr(1)–C(23)	2.263(2)	Zr(1)–C(23)	2.2910(16)
N(1)–C(11)	1.3328(17)	N(1)–C(11)	1.333(2)	N(1)–C(11)	1.341(3)
N(1)–C(13)	1.4640(17)	N(1)–C(13)	1.462(2)	N(1)–C(13)	1.454(3)
N(2)–C(11)	1.3355(16)	N(2)–C(11)	1.342(2)	N(2)–C(11)	1.330(3)
N(2)–C(17)	1.4851(16)	N(2)–C(18)	1.485(2)	N(2)–C(20)	1.486(2)
<i>Bond angles</i>					
C(11)–N(1)–C(13)	122.70(12)	C(11)–N(1)–C(13)	122.46(16)	C(11)–N(1)–C(13)	122.14(19)
C(11)–N(1)–Zr(1)	94.37(8)	C(11)–N(1)–Zr(1)	88.05(10)	C(11)–N(1)–Zr(1)	94.42(12)
C(13)–N(1)–Zr(1)	136.58(9)	C(13)–N(1)–Zr(1)	133.00(12)	C(13)–N(1)–Zr(1)	136.71(16)
C(11)–N(2)–C(17)	124.27(11)	C(11)–N(2)–C(18)	124.72(16)	C(11)–N(2)–C(20)	125.07(17)
C(11)–N(2)–Zr(1)	92.67(8)	C(11)–N(2)–Zr(1)	90.79(11)	C(11)–N(2)–Zr(1)	93.11(12)
C(18)–N(2)–Zr(1)	139.18(8)	C(18)–N(2)–Zr(1)	140.96(12)	C(20)–N(2)–Zr(1)	139.50(14)
Zr(1)–N(1)–C(11) and Zr(1)–N(2)–C(11)	14.9	Zr(1)–N(1)–C(11) and Zr(1)–N(2)–C(11)	33.6	Zr(1)–N(1)–C(11) and Zr(1)–N(2)–C(11)	18.1

processes involving the methyl substituents on the phenyl rings. Schrock et al. [10] have previously seen decomposition through similar types of C–H activation of mesityl substituents in their cationic initiators.

3.4. Polymerization of 1-hexene by initiators **2a–g**

Table 3 presents the results of a study of 1-hexene polymerization by initiators **2a–g** that was conducted at $-10\text{ }^{\circ}\text{C}$. Where polymer was obtained, this table also presents the mean average molecular weight, M_n , and polydispersity, M_w/M_n , of the material as obtained by GPC analysis and the microstructure of the poly(1-hexene) as revealed by ^{13}C NMR spectroscopy [4a]. Using the results obtained with **1a** as a point of reference, it can be clearly seen that the benzyl-substituted initiator **1d** behaves in a nearly identical fashion by quantitatively providing isotactic poly(1-hexene) of similar M_n and M_w/M_n values. Although we have not carried out a kinetic evaluation of 1-hexene polymerization using **1d**, we are confident that, as found for **1a**, polymerizations are living with this initiator under these specific conditions. In contrast to the high activities expressed by **1a** and **1d** where 1-hexene polymerizations are complete within 2 h at $-10\text{ }^{\circ}\text{C}$ (90–95% isolated yields), the polymerization mediated by **1b** is considerably more sluggish as evidenced by both a low 57% yield of isolated material that possesses a correspondingly much lower M_n value (see Table 3). Interestingly, while the narrow polydispersity that is observed with this initiator is indicative that polymerizations with **1b** are also living, it was surprising to find that an atactic polymer microstructure is now obtained. For **1d** and **1g**, significant steric congestion within the ligand environ-

ment most likely plays a key role in shutting down activity, while for **1e**, intramolecular coordination of the chlorobenzyl substituent may be responsible for blocking olefin binding. Finally, for initiator **1f**, which is unstable at $-10\text{ }^{\circ}\text{C}$ in the absence of olefin, a high yield of isotactic poly(1-hexene) can still be obtained, but as the polydispersity value reveals, this polymerization is no longer living.

4. Conclusions

The present structure/activity study serves to show how subtle differences in the ligand environment of the amidinate-based family of Ziegler–Natta initiators derived from **1** can have a profound influence on both activity and the degree of stereocontrol that can be obtained. Surprisingly, it was found that while the benzyl substituent of **2d** can adopt a conformation that apparently does not interfere with the nature of the olefin binding site established by **2a** (i.e. with respect to both the direction of site-isomerization and the level of non-bonded steric interactions with the bound olefin), an isobutyl substituent cannot. Importantly, we believe that the loss of stereocontrol that is observed in the latter case with **2b** is due to the site-isomerization process that no longer has a clear discriminating choice of placing the growing polymer chain towards one amidinate substituent or the other, which in turn leads to promiscuous olefin binding and an atactic polymer microstructure. The present study has also served to further outline the steric limitations of the amidinate substituents and their ability to engage in either intramolecular coordination to the electron-deficient

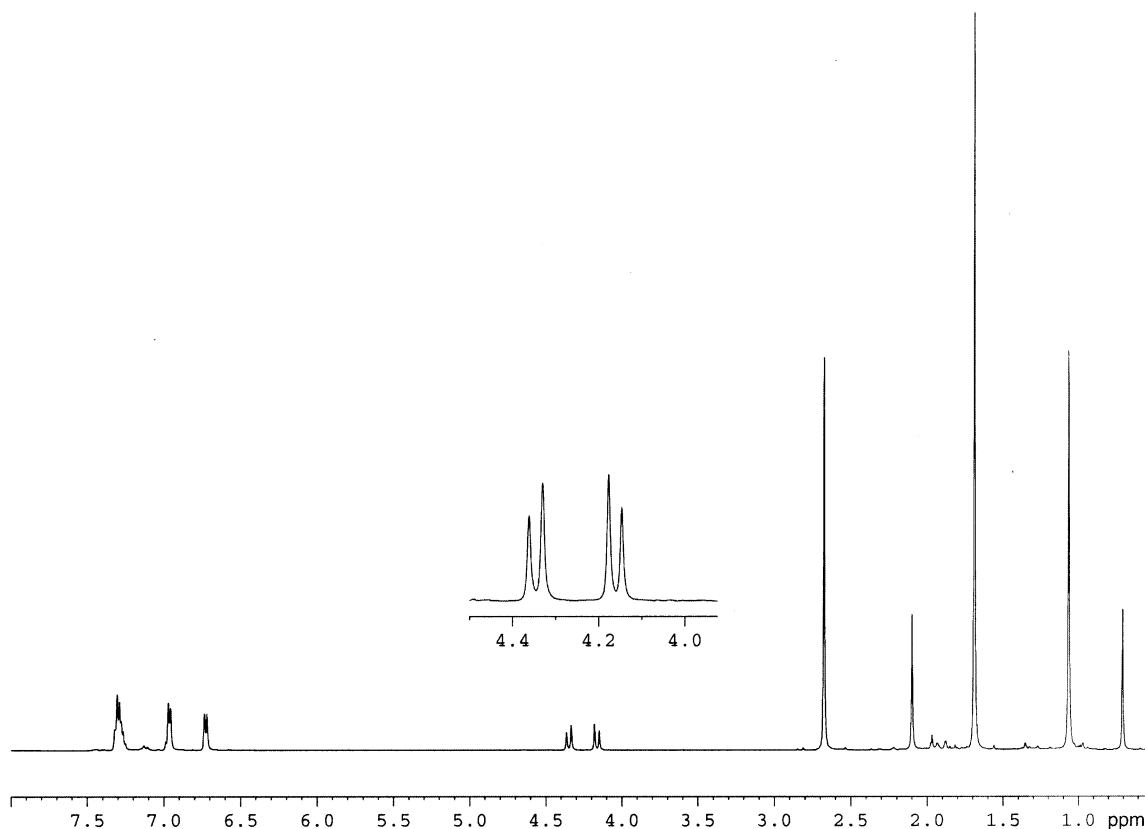


Fig. 4. ^1H NMR (500 MHz, chlorobenzene- d_5 , -10°C) spectrum of **2d**.

Table 3
Polymerization activity and polymer characteristics for initiators **2a–g**

Initiator	M_n	M_w/M_n	Microstructure ^a
2a	19 800	1.03	isotactic
2b	7940	1.03	atactic
2c	na ^b		
2d	19 340	1.10	isotactic
2e	na		
2f	23 580	1.48	isotactic
2g	na		

^a As determined by ^{13}C NMR (100 MHz, CDCl_3 , 25°C) spectroscopy.

^b Not active.

metal center or in undesirable and terminating C–H activation processes.

5. Supplementary material

Crystallographic data (excluding structure factors) for the structures in this paper have been deposited with the Cambridge Crystallographic Data Centre, CCDC Nos. 197488–197490 for compounds **1b**, **1c** and **1d**, respectively. Copies of this data can be obtained free of charge from The Director, CCDC, 12 Union

Road, Cambridge CB2 1EZ, UK (fax: +44-1223-336-033; e-mail: deposit@ccdc.cam.ac.uk or www: <http://www.ccdc.cam.ac.uk>).

Acknowledgements

This work was supported by the National Science Foundation (CHM-0092493) for which we are grateful.

References

- [1] J.D. Scollard, D.H. McConville, *J. Am. Chem. Soc.* 118 (1996) 10008.
- [2] R. Baumann, W.M. Davis, R.R. Schrock, *J. Am. Chem. Soc.* 119 (1997) 3830.
- [3] (a) E.Y. Tshuva, I. Goldberg, M. Kol, *J. Am. Chem. Soc.* 122 (2000) 10706;
(b) J. Tian, P.D. Hustad, G.W. Coates, *Angew. Chem., Int. Ed. Engl.* 39 (2000) 3626;
(c) J. Saito, M. Mitani, J. Mohri, Y. Yoshida, S. Matsui, S. Ishii, S. Kojoh, N. Kashiwa, T. Fujita, *Angew. Chem., Int. Ed. Engl.* 40 (2001) 2918;
(d) J. Saito, M. Mitani, J. Mohri, S. Ishii, Y. Yoshida, T. Matsugi, S. Kojoh, N. Kashiwa, T. Fujita, *Chem. Lett.* (2001) 576.
- [4] (a) K.C. Jayaratne, L.R. Sita, *J. Am. Chem. Soc.* 122 (2000) 958;
(b) K.C. Jayaratne, R.J. Keaton, D.A. Henningsen, L.R. Sita, *J. Am. Chem. Soc.* 122 (2000) 10490;

- (c) R.J. Keaton, K.C. Jayaratne, J.C. Fettinger, L.R. Sita, *J. Am. Chem. Soc.* 122 (2000) 12909;
- (d) R.J. Keaton, K.C. Jayaratne, D.A. Henningsen, L.A. Koterwas, L.R. Sita, *J. Am. Chem. Soc.* 123 (2001) 6197;
- (e) K.C. Jayaratne, L.R. Sita, *J. Am. Chem. Soc.* 123 (2001) 10754.
- [5] K.C. Jayaratne, Y.F. Lam, L.R. Sita, results to be published.
- [6] H.H. Brintzinger, D. Fischer, R. Müllhaupt, B. Rieger, R.M. Waymouth, *Angew. Chem., Int. Ed. Engl.* 34 (1995) 1143.
- [7] (a) J.A. Ewen, *J. Mol. Catal. A: Chem.* 128 (1998) 103;
(b) M.A. Giardello, M.S. Eisen, C.L. Stern, T.J. Marks, *J. Am. Chem. Soc.* 117 (1995) 12114.
- [8] (a) L.R. Sita, J.R. Babcock, *Organometallics* 17 (1998) 5228;
(b) L.A. Koterwas, J.C. Fettinger, L.R. Sita, *Organometallics* 18 (1999) 4183.
- [9] J.R. Babcock, L.R. Sita, *J. Am. Chem. Soc.* 120 (1998) 5585.
- [10] R.R. Schrock, P.J. Bonitatebus, Jr., Y. Schrodi, *Organometallics* 20 (2001) 1056–1058.